International Journal of Computational and Experimental Science and ENgineering (IJCESEN)

Vol. 12-No.3 (2026) pp. 8-13
http://www.ijcesen.com

ISSN: 2149-9144

Research Article

Aeromagnetic and Gamma-Ray Spectrometric Data for Geological Mapping: A Python-Based Automated Workflow Applied to the Djelfa Region, Northern Algeria

Saddek Samai[1], Leila Benhenni[2*]

[1] University of Sciences and Technology Houari Boumediene, Geophysics Department, 16000, Algiers-Algeria
Email: ssamai@usthb.dz - **ORCID:** 0009-0004-7532-8008

[2] University of Sciences and Technology Houari Boumediene, Geophysics Department, 16000, Algiers-Algeria
* **Corresponding Author Email:** lbenhenni@usthb.dz - **ORCID:** 0009-0001-3691-159X

Article Info:

DOI: 10.22399/ijcesen.5312
Received : 25 April 2026
Revised : 05 June 2026
Accepted : 07 June 2026

Keywords

Aeromagnetic;
Gamma-ray spectrometry
EMD micro-levelling
Geological mapping
Northern Algeria
Python; Open-source workflow

Abstract:

This study presents an automated open-source Python-based workflow for the processing and interpretation of airborne geophysical data, applied to the Djelfa region of northern Algeria (R=[4.75°–6.0°E / 34.0°–34.75°N]). The dataset comprises 144,623 measurement points from a legacy airborne survey covering both total magnetic intensity (TMI) and gamma-ray spectrometric channels (K, Th, U). A complete quality control and correction chain was implemented including median statistical levelling, EMD-based micro-levelling, altitude correction and empirical calibration, following IAEA (2003) and Groun et al. (2018). Radiometric crossover RMS errors were reduced by 49.8%, 54.3% and 60.8% for K, Th and U respectively. The processed data were gridded and interpreted through magnetic enhancement filters (HGM, TDR) and spectrometric analysis (RGB ternary composite, K-means classification with five units) to constrain and refine the existing 1:200,000 geological map of the region. TMI gradient analysis delineated major geological contacts consistent with the regional Atlasic tectonic framework. The entire workflow is implemented using open-source Python libraries (Verde, Harmonica, PyEMD, scikit-learn, Matplotlib) and is fully reproducible.

1. Introduction

Airborne geophysical surveys combining magnetic and gamma-ray spectrometric measurements represent one of the most efficient tools for regional geological mapping, particularly in areas where ground access is limited or geological complexity is high. In Algeria, extensive airborne surveys were conducted during the 1970s under the ORGM/SONAREM program, generating a vast archive of magnetic and radiometric data covering most of the national territory. Despite the potential scientific and economic value of these datasets, their exploitation has been limited by data quality issues inherent to the technological constraints of the era, including uncalibrated spectrometers, incomplete background corrections, and significant line-to-line noise (Allek et al., 2025).

Recent advances in open-source scientific computing — particularly the Python ecosystem — now offer powerful tools for systematic reprocessing of such legacy datasets in a transparent, reproducible manner. Libraries such as Harmonica (Uieda et al., 2020), Verde (Uieda et al., 2018) and scikit-learn (Pedregosa et al., 2011) provide functionality equivalent to commercial software, enabling complete geophysical processing workflows without proprietary dependencies.

The Djelfa region of northern Algeria, situated at the boundary between the South Atlas Fold Belt and the Saharan Platform, represents a geologically complex and economically significant area whose subsurface structure remains incompletely characterized. The present study applies a complete Python-based processing and interpretation workflow to airborne magnetic and gamma-ray spectrometric data of this region, with the aim of refining the existing 1:200,000 geological map through geophysical constraints. The region was selected for its key geodynamic position at the Atlas–Saharan Platform boundary, its dense

airborne coverage (144,623 points), and the lithological diversity that makes it a suitable test case for the proposed workflow.

2. Geological setting

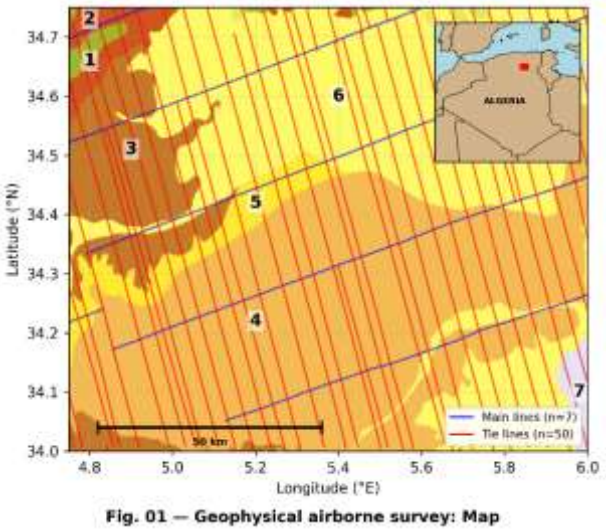

Figure 1. *Djelfa airborne survey flight line map overlaid on the 1:200,000 geological map. Blue: main lines (160°); red: tie lines (340°). Geological units: 1-Upper Cretaceous, 2-Lower Eocene, 3-Middle Eocene, 4-Upper Eocene, 5-Pliocene, 6-Quaternary, 7-Recent.*

The study area is located in the northern Saharan Atlas, encompassing the eastern Djelfa wilaya and western M'Sila wilaya between 4.75°E–6.0°E and 34.0°N–34.75°N. This zone straddles two major geodynamic domains: the South Atlas Fold Belt to the north, characterized by NE-SW trending Atlasic fold structures of Jurassic to Cretaceous age, and the Saharan Platform to the south, representing the stable northern margin of the African craton. The boundary between these two domains is marked by the South Atlas Fault Zone (SAFZ), a major crustal discontinuity with a long polyphase tectonic history (Bracène & Frizon de Lamotte, 2002).

Seven lithostratigraphic units are identified on the 1:200,000 geological map: Upper Cretaceous carbonates (1), Lower Eocene limestones (2), Middle Eocene marls and limestones (3), Upper Eocene formations (4), Pliocene detrital sequences (5), Quaternary alluvial deposits (6), and Recent deposits (7). The Cretaceous units dominate the northwestern sector, while Eocene sequences cover the central and southern portions of the study area.

3. Data and study area

The airborne geophysical database used in this study is part of the national ORGM airborne survey archive of Algeria, stored in SQLite format. Data for the study region were extracted using a spatial query covering the bounding box [4.75°–6.0°E / 34.0°–34.75°N], yielding 147,961 measurement points distributed along 121 flight lines comprising 62 main lines (160° azimuth) and 59 tie lines (340° azimuth). The survey was conducted at a nominal altitude of 150 m above ground level, with a mean measured altitude of 152 m (std=10 m). Along-line point spacing averages 47 m, corresponding to a sampling density appropriate for geological mapping at 1:100,000 to 1:200,000 scale.

Recorded channels include total magnetic intensity (TMI, nT), potassium (K, cps), equivalent uranium (U, cps) and equivalent thorium (Th, cps), as well as flight altitude, line number, azimuth and fiducial index. The geological reference map used for interpretation is the official 1:200,000 geological map of Algeria (ORGM/CGS). The refined dataset, exported as Djelfa_Refined_Final.csv, comprises 144,623 points after removal of flat calibration lines, with channels: TMI anomaly (nT), K (%), Th (ppm), U (ppm) and total count CT (ppm).

4. Processing methodology

4.1 Basic Quality Control

Initial quality control removed measurement points presenting anomalous values: zero TMI readings, altitude below 50 m or above 500 m, and physically impossible potassium values. The retained dataset was subsequently clipped to the study region, yielding 147,961 measurement points. Additionally, 24 flat calibration and ferry lines (standard deviation < 2 nT for TMI) were identified and removed prior to magnetic gridding, leaving 144,623 points in the final refined dataset.

4.2 Magnetic Processing

The TMI anomaly was computed by removing a two-dimensional first-degree polynomial regional trend fitted to the levelled total field, yielding residuals centered around zero (mean = -1.7 nT, std = 28.1 nT). The anomaly field ranges from -86.6 to +85.9 nT, consistent with expected amplitudes for crustal sources at survey altitude in this geological setting. An FFT-based directional decorrugation filter (cutoff frequency = 0.05) was applied along the flight line direction (160°) to remove residual high-frequency noise perpendicular to the flight lines, following Minty (1991).

4.3 Spectrometric Processing

The spectrometric processing chain followed IAEA (2003) guidelines and comprised four sequential steps applied to the K, Th and U channels.

4.3.1 Median Statistical Levelling

Crossover analysis using a 2D nearest-neighbor search in UTM coordinates (tolerance = 500 m) identified 265 crossover pairs across 55 main lines and 46 tie lines. Median statistical levelling reduced crossover RMS errors by 12.4%, 7.2% and 34.2% for K, Th and U respectively, following the approach of Groun et al. (2018).

4.3.2 EMD Micro-levelling

Empirical Mode Decomposition (EMD) micro-levelling was applied along each flight line following Groun et al. (2018). Testing of n = 1 to 4 IMFs showed that n = 2 provided the optimal balance between noise reduction and geological signal preservation, with variance removed of 39.8%, 55.4% and 51.9% for K, Th and U. Total improvements from raw data reached 49.8%, 54.3% and 60.8% for K, Th and U respectively.

4.3.3 Altitude Correction

Altitude correction normalized all radiometric measurements to a reference height of 60 m following IAEA (2003), using standard atmospheric attenuation coefficients: $\mu K = 0.00350$ m^{-1}, $\mu Th = 0.00335$ m^{-1}, $\mu U = 0.00340$ m^{-1}. At mean survey altitude of 152 m, corrections increased mean count rates by approximately 37% across all channels.

4.3.4 Calibration

Sensitivity coefficients were derived empirically by normalizing mean count rates after altitude correction to target crustal averages of 2.0%, 8.0 ppm and 2.0 ppm for K, Th and U respectively, consistent with IAEA (2003) guidelines for sedimentary-dominated terranes.

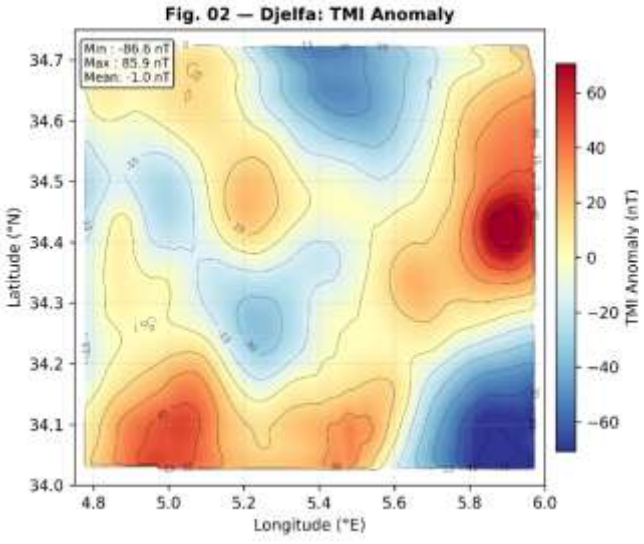

Figure 2. *TMI anomaly map after 2D polynomial regional trend removal and FFT decorrugation. Contour interval: 10 nT.*

Final calibrated values (K: mean=2.00%, std=0.29%; Th: mean=8.00 ppm, std=3.13 ppm; U: mean=2.00 ppm, std=0.61 ppm) are consistent with crustal averages for northern Algeria.

5. Magnetic interpretation

The TMI anomaly map (Fig. 02) reveals a complex pattern of positive and negative anomalies reflecting the heterogeneous nature of the subsurface magnetic sources in the Djelfa region. The anomaly field ranges from -86.6 to +85.9 nT around a near-zero mean (-1.7 nT), confirming the effectiveness of the regional trend removal.

Two major positive anomaly domains are identified. The southwestern domain, centred around 5.0°E/34.3°N, exhibits amplitudes exceeding +60 nT and is interpreted as reflecting a shallow magnetic source, likely a mafic intrusive body or a basement uplift. The northeastern domain, centred around 5.8°E/34.4°N, presents a more circular anomaly (~+40 nT), consistent with a discrete buried intrusive body. These two positive domains are separated by a broad NE-SW trending negative zone (-40 to -60 nT) interpreted as a structural depression with low-susceptibility fill.

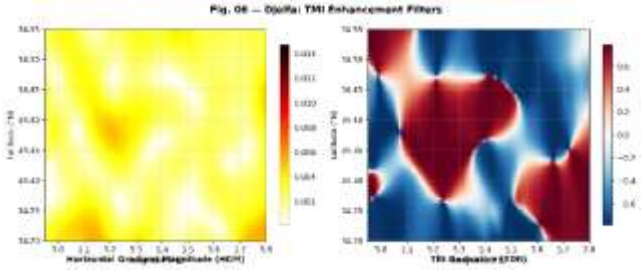

Figure 3. *TMI enhancement filters: (left) HGM highlighting lithological contacts; (right) TDR delineating magnetic source edges. White band = TDR zero-crossing.*

Enhancement filters (Fig. 06) provide additional structural constraints. The Horizontal Gradient Magnitude (HGM) delineates zones of maximum lateral magnetization contrast corresponding to lithological contacts. The Tilt Derivative (TDR) zero-crossings (Miller & Singh, 1994) reveal a major NE-SW trending structural boundary at approximately 5.2–5.3°E. This lineament is interpreted as a significant geological contact between contrasting lithological units; it is noteworthy that no mapped fault appears on the existing 1:200,000 geological map within the study area boundaries. Secondary NW-SE lineaments from HGM maxima may represent transverse contacts or transfer zones (Guiraud et al., 1992).

6. Spectrometric interpretation

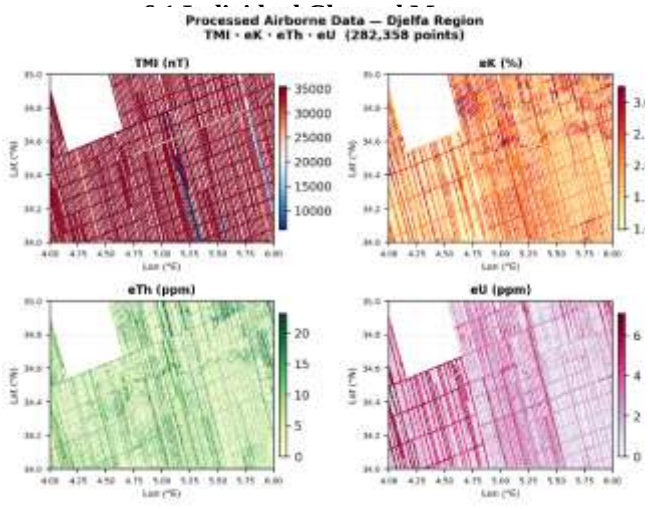

Figure 4a. *Calibrated radiometric maps: (a) K (%), (b) Th (ppm), (c) U (ppm), (d) Total Count CT (ppm). Gaussian smoothed (σ=5).*

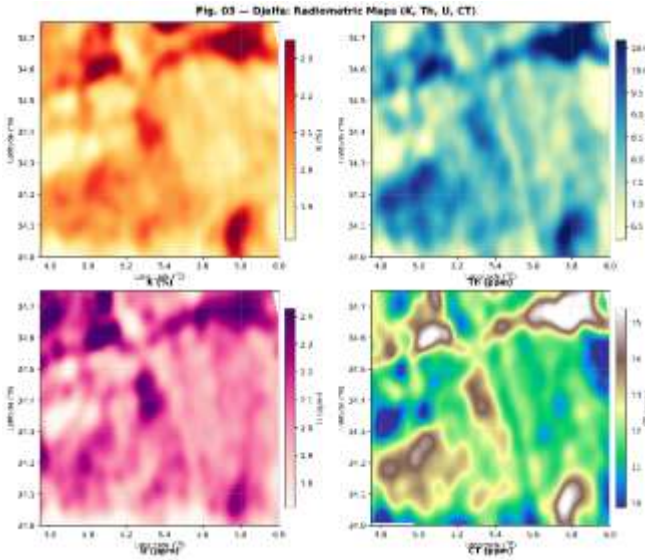

Figure 4b. *Processed radiometric maps: (a) K (%), (b) Th (ppm), (c) U (ppm), (d) Total Count CT (ppm). Gaussian smoothed (σ=5).*

The calibrated radiometric maps (Fig. 03) reveal systematic spatial variations in K, Th and U reflecting the surface lithological diversity. The potassium map shows relatively homogeneous values (mean 2.00%, std 0.29%) with elevated concentrations in the northwestern sector corresponding to Cretaceous outcrops. The thorium map exhibits the highest spatial variability (mean 8.00 ppm, std 3.13 ppm), providing the clearest lithological discrimination, with high Th (>10 ppm) in the northwestern Cretaceous formations consistent with heavy mineral enrichment (Wilford et al., 1997). Localized high-U zones suggest uranium mobility through oxidizing fluids, possibly associated with phosphatic horizons or structural discontinuities (Amara et al., 2017).

6.2 RGB Ternary Composite

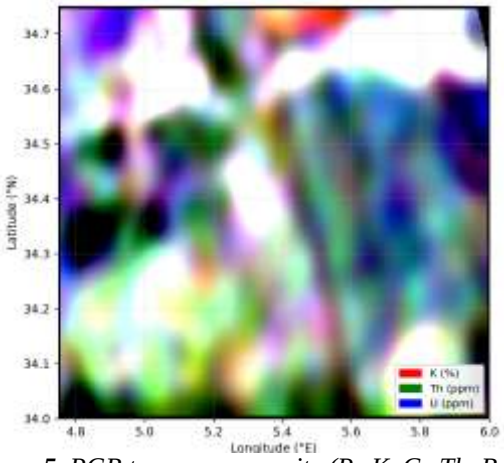

Figure 5. *RGB ternary composite (R=K, G=Th, B=U) following IAEA (2003) convention.*

The RGB ternary composite (Fig. 04), constructed by assigning K to red, Th to green and U to blue following IAEA (2003) convention, provides an effective visualization of lithological diversity. The northwestern sector shows green tones (Th-rich Cretaceous), the central region orange-yellow tones (balanced K-Th Eocene sequences), and localized blue patches indicate U enrichment zones. White areas represent balanced K-Th-U distributions typical of the carbonate platform facies.

6.3 Radiometric Classification

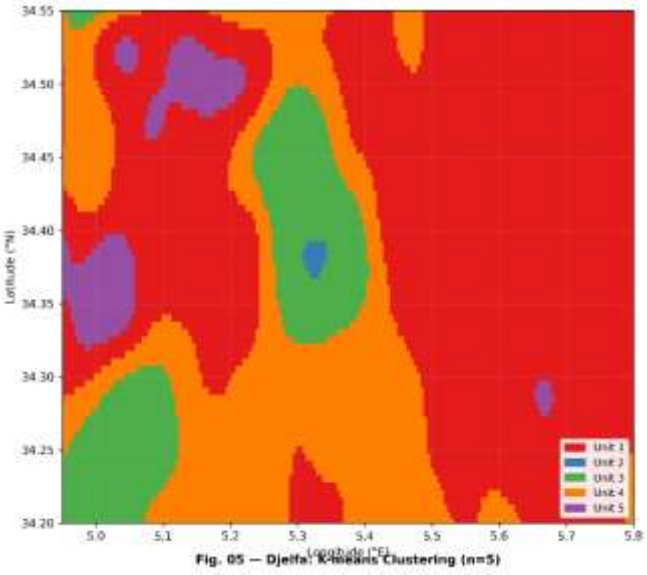

Figure 6. *K-means clustering map (n=5) of standardized K-Th-U data. Five units reflect main lithological formations.*

Unsupervised classification of the radiometric dataset was performed using the K-means algorithm (MacQueen, 1967). The optimal number of classes (K=5) was determined by minimizing the within-class variance while maximizing the between-class separation, consistent with the five lithostratigraphic units of the 1:200,000 geological

map. The inertia curve confirmed this choice, showing significant reduction in within-class variance up to K=5, beyond which additional classes yield marginal improvement. Unit 1 (dominant) represents the Eocene carbonate platform. Unit 2 corresponds to high-U phosphatic horizons. Unit 3 shows elevated Th associated with Cretaceous outcrops. Unit 4 represents mixed Eocene sequences. Unit 5 corresponds to Quaternary cover. The spatial distribution shows good correspondence with the geological map boundaries (Wilford et al., 1997).

7. Geological map refinement

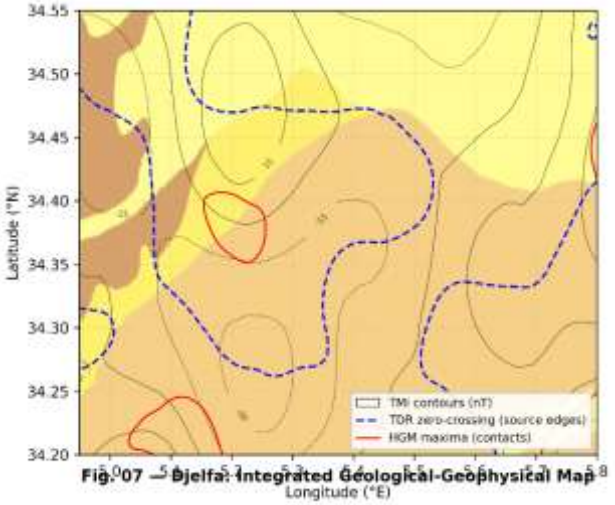

Figure 7. *Geological-geophysical map combining geological map background with TMI contours (black), TDR zero-crossings (blue dashed) and HGM contacts*

The geophysical map (Fig. 07), combining TMI anomaly contours, TDR zero-crossing lineaments and HGM contact zones overlaid on the 1:200,000 geological map, reveals structural and lithological elements that complement the existing geological interpretation. (red). Major NE-SW geophysical lineament at 5.2–5.3°E interpreted as a significant lithological contact.

The most significant finding is the identification of a major NE-SW trending geophysical lineament at approximately 5.2–5.3°E, delineated by both TDR zero-crossing and HGM maxima. This lineament cuts across several mapped geological units and is interpreted as the surface expression of a significant lithological contact or deep-seated structural discontinuity. No mapped fault — including the South Atlas Fault Zone — appears on the existing geological map within the study area; the geophysical signature suggests a fundamental lithological contrast warranting further ground investigation.Secondary NW-SE lineaments from HGM maxima are interpreted as transverse contacts, possibly reflecting reactivated basement structures that influenced the geometry of the overlying Mesozoic-Cenozoic cover (Guiraud et al., 1992). The southwestern positive magnetic anomaly suggests a buried mafic intrusive body at depth, analogous to similar occurrences in the western Saharan Atlas (Amara et al., 2017). The high-Th radiometric unit (Unit 3) provides the clearest discrimination of the Cretaceous outcrops in the northwestern sector.

8. Conclusions

This study presented a complete, reproducible Python-based workflow for processing and interpretation of legacy airborne geophysical data applied to the Djelfa region. The main conclusions are:

(1) The processing chain reduced radiometric crossover RMS errors by 49.8%, 54.3% and 60.8% for K, Th and U respectively, demonstrating the effectiveness of EMD micro-levelling for legacy NaI detector datasets.

(2) TMI gradient analysis (HGM, TDR) delineated a major NE-SW geological contact at 5.2–5.3°E not represented on the existing 1:200,000 geological map, together with secondary NW-SE transverse features and a buried mafic source in the southwestern sector.

(3) RGB ternary composite and K-means clustering identified five spectrometric units correlating with the mapped geological formations, with thorium providing the most effective lithological discriminator.

(4) The entire workflow is implemented in open-source Python (Verde, Harmonica, PyEMD, scikit-learn, Matplotlib) and is fully reproducible, providing a methodological template applicable to similar legacy airborne datasets across Algeria.

Author Statements:

- **Ethical approval:** The conducted research is not related to either human or animal use.
- **Conflict of interest:** The authors declare that they have no known competing financial interests or personal relationships that could have appeared to influence the work reported in this paper
- **Acknowledgement:** The authors declare that they have nobody or no-company to acknowledge.
- **Author contributions:** The authors declare that they have equal right on this paper.

- **Funding information:** The authors declare that there is no funding to be acknowledged.

- **Data availability statement:** The data that support the findings of this study are available on request from the corresponding author. The data are not publicly available due to privacy or ethical restrictions.
- **Use of AI Tools:** The author(s) declare that no generative AI or AI-assisted technologies were used in the writing process of this manuscript.

References

1. Allek, K., Zeghouane, H., Hamoudi, M. & Groun, D. (2025). Improving Data Quality of an Old Airborne Geophysical Survey to Support Geological Mapping: A Case Study in Tahifet Region, Hoggar (Algeria). Springer, pp.105–123.
2. Amara, M., Hamoudi, M. et al. (2017). New insight of geological structures of Ahnet and northwestern Tin Zaouatine terranes from aeromagnetic, gamma ray and remote sensing data. Arabian Journal of Geosciences, 10, 1–20.
3. Blakely, R.J. (1995). Potential Theory in Gravity and Magnetic Applications. Cambridge University Press.
4. Bracène, R. & Frizon de Lamotte, D. (2002). The origin of intraplate deformation in the Atlas system of western and central Algeria. Tectonophysics, 357, 207–226.
5. Dickson, B.L. & Scott, K.M. (1997). Interpretation of aerial gamma-ray surveys. AGSO Journal, 17(2), 187–200.
6. Grasty, R.L. (1997). Radon emanation and soil moisture effects on airborne gamma ray measurements. Geophysics, 62(5), 1379–1385.
7. Groun, D., Allek, K. & Bouguern, A. (2018). Statistical approach for microleveling of aerogeophysical data. Journal of Applied Geophysics, 159, 418–428.
8. Guiraud, R., Bellion, Y., Benkhelil, J. & Moreau, C. (1992). Post-Hercynian tectonics in northern and western Africa. Geological Journal, 27, 433–466.
9. IAEA (2003). Guidelines for Radioelement Mapping Using Gamma Ray Spectrometry Data. IAEA-TECDOC-1363, Vienna, 173p.
10. Luyendyk, A.P.J. (1997). Processing of airborne magnetic data. AGSO Journal, 17(2), 31–38.
11. Miller, H.G. & Singh, V. (1994). Potential field tilt — a new concept for location of potential field sources. Journal of Applied Geophysics, 32, 213–217.
12. Minty, B.R.S. (1991). Simple micro-levelling for aeromagnetic data. Exploration Geophysics, 22, 591–592.
13. Minty, B.R.S., Luyendyk, A.P.J. & Brodie, R.C. (1997). Calibration and data processing for airborne gamma-ray spectrometry. AGSO Journal, 17, 51–62.
14. Pedregosa, F. et al. (2011). Scikit-learn: Machine learning in Python. JMLR, 12, 2825–2830.
15. Roest, W.R., Verhoef, J. & Pilkington, M. (1992). Magnetic interpretation using 3D analytic signal. Geophysics, 57, 116–125.
16. Uieda, L. et al. (2018). Verde: Processing and gridding spatial data using Green's functions. JOSS, 3(29), 948.
17. Uieda, L. et al. (2020). Harmonica: Forward modeling and inversion of gravity and magnetic data. JOSS, 5(52), 2168.
18. Verduzco, B., Fairhead, J.D., Green, C.M. & MacKenzie, C. (2004). New insights into magnetic derivatives. The Leading Edge, 23, 116–119.
19. MacQueen, J. (1967). Some methods for classification and analysis of multivariate observations. Proceedings of the 5th Berkeley Symposium on Mathematical Statistics and Probability, 1, 2812013297.
20. Wessel, P. et al. (2019). The Generic Mapping Tools Version 6. G-cubed, 20, 5556–5564.
21. Wilford, J.R., Bierwirth, P.N. & Craig, M.A. (1997). Application of airborne gamma-ray spectrometry in soil/regolith mapping. AGSO Journal, 17(2), 201–216.